Chemical Engineering Journal 227 (2013) 56–65

Contents lists available at SciVerse ScienceDirect

Chemical Engineering Journal

journal homepage: www.elsevier.com/locate/cej

Evidence of wettability variation on carbon nanofiber layers grown on oxidized silicon substrates

H. Nair [a], R.M. Tiggelaar [b], D.B. Thakur [a], J.G.E. Gardeniers [b], A. van Houselt [a,*], L. Lefferts [a]

[a] Catalytic Processes and Materials, MESA+ Institute for Nanotechnology, University of Twente, PO Box 217, 7500 AE Enschede, The Netherlands
[b] Mesoscale Chemical Systems, MESA+ Institute for Nanotechnology, University of Twente, PO Box 217, 7500 AE Enschede, The Netherlands

HIGHLIGHTS

- Carbon nano fibers (CNFs) were grown on Si based Ni thin films.
- Adhesion of the CNFs varies with oxidation state and composition of the substrate.
- We characterized the wettability (water contact angle) on this surfaces.
- The wettability varies between superhydrophobic and slightly hydrophilic.

GRAPHICAL ABSTRACT

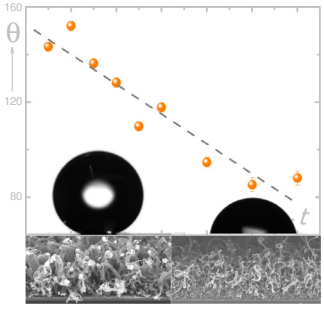

ARTICLE INFO

Article history:
Available online 2 November 2012

Keywords:
Carbon nanofiber growth
Tunable wettability
Superhydrophobicity
Microfluidic devices

ABSTRACT

This paper describes how layers of carbon nanofibers (CNFs) with a controllable wettability can be synthesized by means of thermal catalytic chemical vapor deposition on nickel-based thin films on oxidized silicon supports. In order to achieve well-adhesive CNF-layers with a uniform surface coverage and tunable wettability without the necessity of post-synthesis treatments, a series of synthesis parameters is investigated: the pretreatment atmosphere (hydrogen or oxygen; 2 h, 500 °C), the use of ethylene (C_2H_4) or an ethylene/hydrogen (C_2H_4/H_2) mixture as hydrocarbon source, and the growth time (in the range 5–60 min).

Fast and uniform CNF-growth is found on reduced Ni-based thin films using C_2H_4/H_2 at a synthesis temperature of 635 °C. The CNF-layers on Ni are superhydrophobic or highly hydrophobic for all growth times, but their adhesion to the support is poor for growth times >30 min. In contrast, the adhesion of CNF-layers on Ni/Ta is excellent. Moreover, the wettability of these as-synthesized CNF-layers can be controlled by variation of the growth time: from superhydrophobic ($\leqslant$10 min) to hydrophilic ($\geqslant$50 min). CNF-layers with such tunable wettability can be easily integrated in flow channels of silicon-based microfluidic systems, thereby offering numerous applications.

1. Introduction

Surface wettability is of key importance in a myriad of applications [1–7]. Especially hydrophobic surfaces are both technologically [4–7] and fundamentally [8,9] interesting. Superhydrophobic surfaces (contact angle >150°) have been used to enhance mixing and drug delivery [2]. Other applications of hydrophobic layers are self-cleaning surfaces [3], anti-freezing surfaces [4], slip enhancement [5,6] and their use for efficient catalytic multiphase microreaction technology [7]. Wetting (hydrophilic) surfaces obey the no-slip boundary conditions, whereas non-wetting (hydrophobic) surfaces exhibit apparent slip of the order of microns [8].

The aspect of reducing drag at the liquid–solid boundary is of importance for the efficiency of microfluidic systems. Mass transport in microfluidic devices, systems comprising enclosed flow channels with a high surface-to-volume ratio, is heavily influenced by viscous forces, that are mainly determined by the properties of the liquid–solid interface. When the solid has a water wetting surface, the linear velocity of the fluid at the interface is reduced to

* Corresponding author.
E-mail address: a.vanhouselt@utwente.nl (A. van Houselt).

1385-8947/$ - see front matter © 2012 Elsevier B.V. All rights reserved.
http://dx.doi.org/10.1016/j.cej.2012.10.013

zero, resulting in a stagnant fluid layer, and consequently high energy dissipation. When the solid has a hydrophobic surface, the linear velocity of the fluid at the interface will be non-zero, which, in turn, will lower the energy dissipation due to drag.

Superhydrophobic surfaces (and to a less extent hydrophobic surfaces) combine a microstructured surface with a low surface energy [9]. In general, microstructures can be obtained by lithography [10], etching, electro-spinning, electrochemical reactions and sol–gel processing [11], particle deposition [12], or chemically grown carbonaceous nanostructures [13]. These nanostructures can, based on their geometry, be classified as carbon nanotubes (CNTs) or CNFs. Single or multi-walled CNTs are formed by one or more concentrically rolled graphene sheet(s), thus forming mainly straight hollow cylinders. When the graphene sheets have an angle with respect to the main axis the resulting structures are CNFs. CNTs and CNFs can grow in two orientations with respect to their support: parallel aligned ('straight'), or randomly-oriented ('entangled') [14].

In order to achieve superhydrophobicity, usually aligned CNTs (aCNTs) are chemically modified after synthesis, for example by coatings of fluoroalkylsilanes or thiols [15–18]. In a few cases, superhydrophobicity of pristine aCNTs is reported [19–22], and for CNFs superhydrophobicity of as-grown structures is rarely reported [23–25].

Goal of this work is to fabricate CNF-layers on Ni-based thin film coatings on oxidized silicon supports that have good adhesive properties, uniform surface coverage and tunable wettability without any post-synthesis treatment, and thus could be integrated in microfluidic devices. The method used is thermal catalytic chemical vapor deposition (TC–CVD), and a series of synthesis parameters is systematically varied. The TC–CVD growth settings are applied to different nickel configurations, i.e. 10 nm Ni, 25 nm Ni, and 25 nm Ni/10 nm Ta. The parameters that are studied are the pretreatment atmosphere (hydrogen or oxygen; 2 h, 500 °C), the use of ethylene (C_2H_4) or ethylene/hydrogen (C_2H_4/H_2) as hydrocarbon source (synthesis temperature 635 °C), and the growth time (in the range 5–60 min). By varying the growth time on reduced Ni/Ta on oxidized silicon, we show that the wettability of well-adhesive, as-synthesized CNF-layers (635 °C, C_2H_4/H_2) can be tuned from superhydrophobic to hydrophilic.

2. Experimental

2.1. Preparation of nickel-based thin films on oxidized silicon substrates

On silicon substrates ((100)-orientation, p-type, single-side polished, 100 mm diameter, 525 ± 25 μm thickness, resistivity 5–10 Ω cm; Okmetic, Finland) a 250 nm thick SiO_2 layer was grown *via* wet oxidation (45 min, 1000 °C). By means of standard UV-lithography a pattern was defined in spin-coated photoresist (Olin, 906-12), resulting in unmasked squares of 8 mm × 8 mm onto which nickel-based thin films were deposited *via* electron-beam evaporation. Three different compositions were evaporated: 10 nm nickel (Ni), 25 nm Ni and 25 nm Ni on 10 nm tantalum (Ta). Post to metal deposition, an ultrasonic lift-off step in acetone (>20 min; VLSI 100038, BASF) was performed, followed by further rinsing and spin drying. Finally, the nickel-coated substrates were diced into samples of 1 cm × 1 cm (Disco DAD-321 dicing machine). Details of the sample fabrication procedure can be found elsewhere [26].

2.2. Synthesis of CNFs on Ni-coated samples

Prior to CNF synthesis, the nickel-based thin film samples were ultrasonically cleaned in acetone (10 min, Branson 200 ultrasonic cleaner) and de-ionized water (5 min, 25 °C) to remove organic contaminants, followed by drying with pressurized technical air.

For CNF synthesis, samples were placed centrally on a flat quartz boat inside a quartz reactor and the temperature was increased in nitrogen (N_2; 99.999%, INDUGAS) to 500 °C (5 °C/min). At this temperature the pretreatment was done, in order to dewet the continuous as-evaporated thin film into nickel nanoparticles which are a requirement for catalytic CNF-growth [26,27]. Two pretreatment environments were used: 20 vol.% of hydrogen (H_2; 99.999%, INDUGAS) in N_2 and 20 vol.% of air in N_2, both for 2 h at a total flow rate of 50 ml/min. After this reduction or oxidation pretreatment, the temperature was increased in N_2 (5 °C/min) to the desired CNF-synthesis temperature (635 °C). CNF-synthesis was performed by thermal catalytic chemical vapor deposition of 25 vol.% ethylene (C_2H_4; 99.95% PRAXAIR), with and without addition of 6.25 vol.% H_2, in N_2 (total flow rate 100 ml/min) for various growth times. After the reaction time, the samples were cooled in N_2 (10 °C/min) till room temperature. All flow rates are given under normal conditions (ambient temperature). Post to synthesis, the samples were characterized without additional functionalization of the CNFs.

Three synthesis parameters were varied in order to obtain the formation of well-adhesive CNFs with uniform coverage as well as tunable wettability on the surface of oxidized silicon samples with an evaporated nickel-based thin film: (i) the pretreatment atmosphere (hydrogen or oxygen), (ii) the use of ethylene or ethylene/hydrogen as hydrocarbon source (at 635 °C), and (iii) the synthesis time (in the range 5–60 min).

2.3. Characterization

The synthesized CNF-layers were investigated using high-resolution scanning electron microscopy (HRSEM; LEO 1550) to determine the presence and morphology of CNFs as well as their uniformity in coverage (top view images). Cross-sectional SEM images were used to determine the thickness of the CNF-layers, and their adhesion to the silicon support. CNF-layer thicknesses were determined based on at least three representative images taken from different samples (exposed to identical processing). From each SEM-image 10 thickness measurements were determined using ImageJ software. The reported values are thus averages of $\geqslant$30 measurements, and the standard deviation amounts up to 1.5 μm for the thicker samples.

The adhesion of CNF-layers to the silicon support was also evaluated with fluid flows (air and water flows with a linear velocity of 100 m/s for 5 min and 2 m/s for 1 h, respectively), in combination with weight measurements prior and post to these flow experiments (details in [26]).

Static contact angles were measured using an OCA contact angle meter (Data physics) using high purity milli-Q water (Millipore Synergy® system) at room temperature and a relative humidity of ~33%. A computer controlled Hamilton syringe (500 μL) was used to inject a droplet of water (3 μL). Droplets were placed on at least five different locations of each sample (i.e. samples covered with as-evaporated Ni, pretreated Ni, and CNF-layers), and the contact angle was determined from an elliptical fit through the droplet contour (side view imaging). The reported averaged values have a standard deviation of ±1°.

3. Results and discussion

3.1. Influence of pretreatment atmosphere on CNF synthesis

SEM images of CNFs obtained on oxidation-pretreated and reduction-pretreated samples with 10 nm as-evaporated Ni after

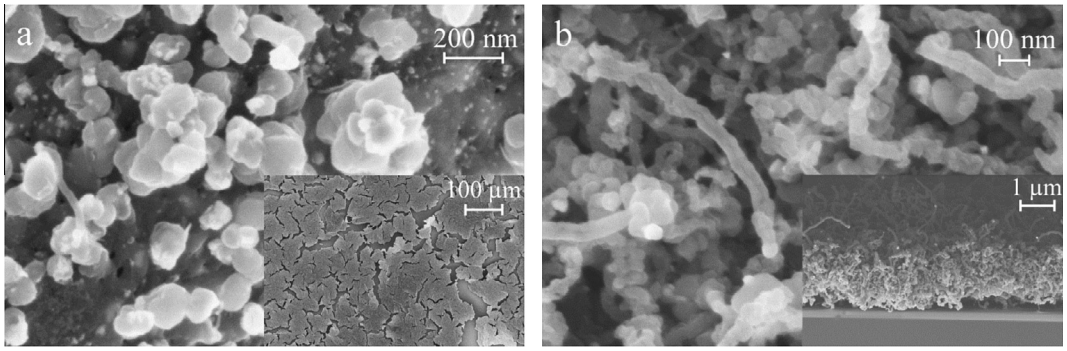

Fig. 1. SEM images of samples with 10 nm Ni after 1 h of CNF growth (635 °C, C_2H_4). Panel (a) shows a top-view of an oxidation-pretreated sample with in the inset a larger field of view and panel (b) shows a top-view of a reduction-pretreated sample with a side-view in the inset.

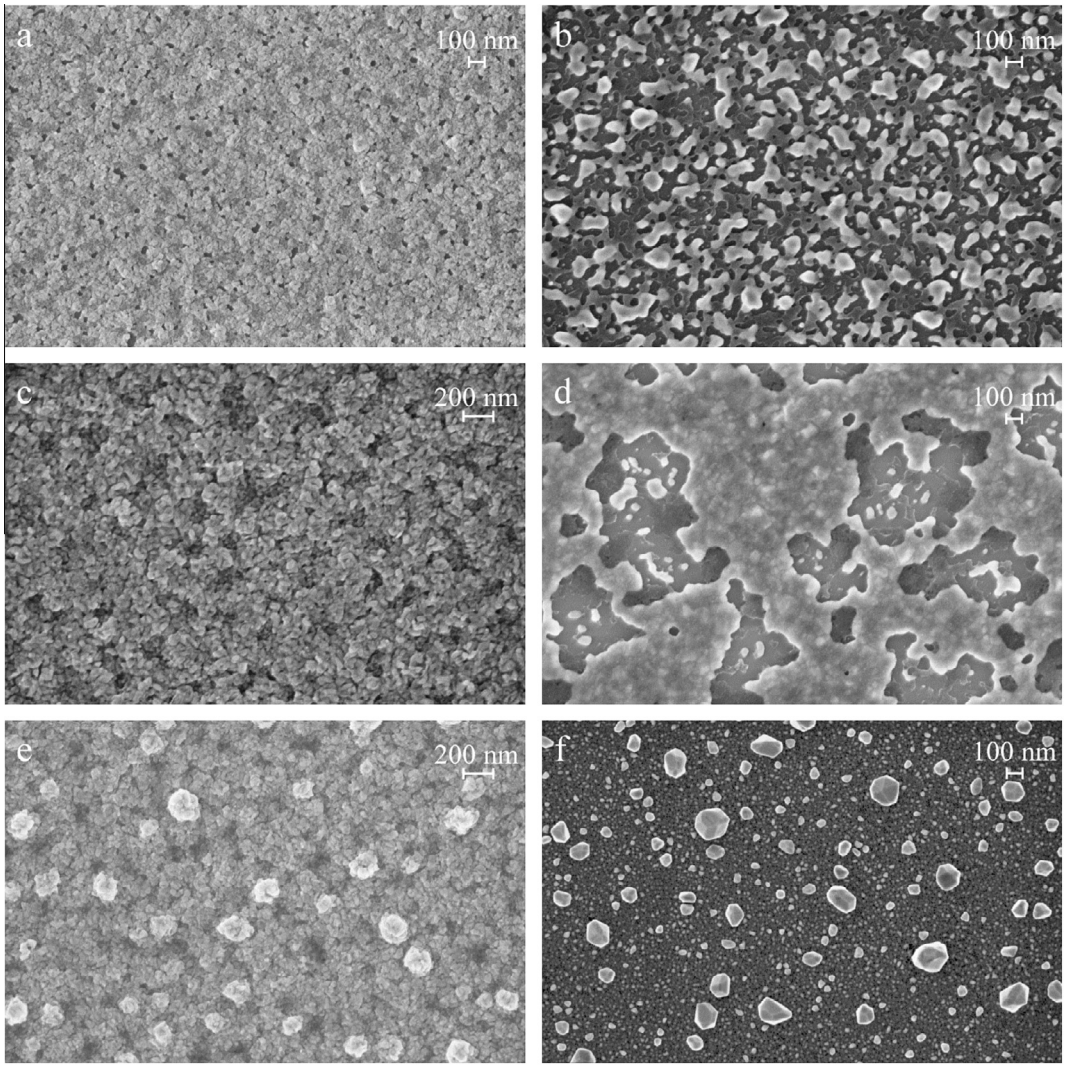

Fig. 2. SEM images of nickel-based thin films after oxidation or reduction pretreatment (2 h, 500 °C, O_2 or H_2): (a) oxidized 10 nm Ni, (b) reduced 10 nm Ni, (c) oxidized 25 nm Ni, (d) reduced 25 nm Ni, (e) oxidized 25 nm Ni/10 nm Ta and (f) reduced 25 nm Ni/10 nm Ta.

a reaction time of 1 h with C_2H_4 at 635 °C are shown in Fig. 1. These synthesis settings yielded a layer with particles of carbon (or carbonaceous species) on the oxidation-pretreated sample (see Fig. 1a), whereas on the reduction-pretreated sample CNFs (visible as wormlike features in Fig. 1b) can be seen, which are equally distributed on the nickel coating.

In more detail, the 10 nm Ni sample that was oxidation-pretreated only occasionally had fibers (approx. 1 fiber per square micrometer with a diameter of ca. 30 nm), and this layer (consisting of carbon and fibers) had a poor adhesion to the surface of the sample, as evidenced by the occurrence of many cracks (inset of Fig. 1a). The formation of carbon deposits on the oxidation-pre-

treated 10 nm Ni coating is, in accordance with [28], attributed to catalyst deactivation (coke formation). In contrast, reduction-pretreated 10 nm Ni samples were covered with many carbon fibers (diameter 30–50 nm). These CNFs were of tip-type growth with small nickel particles at the top of each fiber, and the CNFs showed an entangled morphology. The adhesion of this CNF-layer was rather poor (see inset Fig. 1b: partial detachment of the CNF-layer). Clearly, the pretreatment conditions influence the dewetting of the 10 nm nickel film, and subsequent CNF nucleation and growth.

SEM images of 10 nm Ni, as well as 25 nm Ni and 25 nm Ni/10 nm Ta after oxidation and reduction are shown in Fig. 2.

The as-evaporated continuous Ni-layers dewet into nanoparticles during the oxidation or reduction pretreatment. It can be seen that the pretreatment atmosphere, the thickness of the nickel layer and the use of a Ta adhesion layer influenced the dewetting of the Ni film (in terms of nanoparticle size and distribution, see Fig. 2). The oxidation-pretreated samples appear to be less dewetted than their reduced counterparts (see Fig. 2a, c, e vs. Fig. 2b, d, f). Moreover, the thickness of Ni also influences the rate of dewetting, as can be seen from Fig. 2b and d (10 nm Ni and 25 nm Ni; reduction-pretreated): thinner Ni-layers dewet faster. Clearly, the presence of a Ta adhesion layer favors the formation of nanoparticles (compare Fig. 2e with Fig. 2c and Fig. 2f with Fig. 2d). For all thin films dewetting occurs *via* nucleation of holes or spinodal dewetting, followed by growth of nanoparticles [29–31]. It is known that in an oxygen containing annealing atmosphere the interfacial tension between the support and nanoparticles is lower [27], due to formation of NiO at the surface of the nanoparticles. This decreases the surface mobility and the dewetting process of the nickel film. Under a reducing atmosphere, metals have a weaker interaction with oxidized substrates: hydrogen reduces the oxidized metal surface and, as a result the surface mobility increases, thereby fastening the dewetting process. Thus, for similar as-evaporated thin films dewetting is faster in a reducing atmosphere, as evidenced in Fig. 2.

Reduced 10 nm Ni samples (Fig. 2b) yielded smaller nanoparticles (with spherical or elliptical shape) with a higher areal density compared to 25 nm Ni film samples (Fig. 2d), which is in agreement with our previous studies and literature. In fact, for the used reduction pretreatment conditions the 25 nm Ni did not yet fully dewet into nanoparticles (Fig. 2d), which is in agreement with other studies [27]. The presence of Ta underneath the Ni thin film yielded numerous multifaceted nanoparticles: full dewetting of the 25 nm Ni film (Fig. 2f). This is because on tantalum the surface mobility of nickel is higher, and, hence, the rate of dewetting increases on Ni/Ta compared to a Ni film without an adhesion layer [27]. The Ta layer can be observed as a continuous 'spongy' layer below the Ni particles (Fig. 2f). Depending on the composition of the as-evaporated thin films and pretreatment conditions, the roughness of the as-evaporated films ($\leqslant$2 nm [32]) increases to 60–150 nm after oxidation or reduction [27].

Nickel nanoparticles are a requisite for CNF-synthesis. For samples with 10 nm Ni, 25 nm Ni and 25 nm/10 nm Ta, these nanoparticles are only formed by means of a reduction pretreatment. Indeed, as evidenced in Fig. 1, on oxidation-pretreated Ni-based films nearly no CNF growth has occurred after 1 h synthesis (C_2H_4 at 635 °C), whereas reduction-pretreatment resulted in CNF-formation, independent of the composition of the nickel-based thin film. Cross-sectional SEM images of CNFs on reduced 25 nm Ni and 25 nm Ni/10 nm Ta are shown in Fig. 3 (see Fig. 1b for 10 nm Ni).

CNF-layers synthesized on reduced Ni/Ta have the highest CNF yield, i.e. a thicker CNF-layer, and excellent adhesion to the silicon support material. In case of a 25 nm Ni film without Ta, the weaker adhesion results in the removal of CNFs during sample preparation for the cross-sectional SEM image in Fig. 3b. This is in agreement with previous work on fused silica substrates, which are – from the point-of-view of the composition of the surface on which the Ni-based films are deposited – comparable to oxidized silicon [26]. Exposure to fluid flows revealed that CNF-layers synthesized on Ni/Ta had excellent adhesion (weight loss of the CNF-layers below 6%), whereas CNF-layers on Ni were (nearly) completely flushed away from the support material, indicating poor adhesion. The use of a Ta layer ensures an excellent adhesion of the synthesized CNF-layers to the support, whereas the roughness of the Ni films after pretreatment has no noticable influence on the adhesive quality. Indeed, droplet impact also revealed a difference in adhesion of CNF-layers on Ni/Ta and Ni films (see Section 3.3).

3.2. Influence of hydrogen on CNF synthesis

In Fig. 4, SEM images are shown of CNFs synthesized with a reactant mixture of C_2H_4 and H_2 (1 h, 635 °C) on 10 nm Ni samples exposed to various pretreatment conditions.

Addition of hydrogen to ethylene enhances the growth of carbon nanofibers, and yields uniform coverage of samples with CNFs. The thickness of the CNF-layer has increased with respect to results obtained without H_2 (Fig. 1). This is in agreement with literature: the addition of hydrogen increases the CNF formation rate, resulting in the formation of long, thin fibers by slowing down the catalyst deactivation [33,34]. It is discussed by Chinthaginjala et. al. [34] that the addition of H_2 influences the formation of a CNF layer *via* two effects: (1) H_2 addition decreases the CNF growth rate on active Ni particles, (2) H_2 delays deactivation of nanoparticles (i.e. prevents encapsulation of Ni) which might occur due to excess deposition of carbon *via* decomposition of ethylene, thus leading to thicker CNF layers and hence to a higher CNF formation rate.

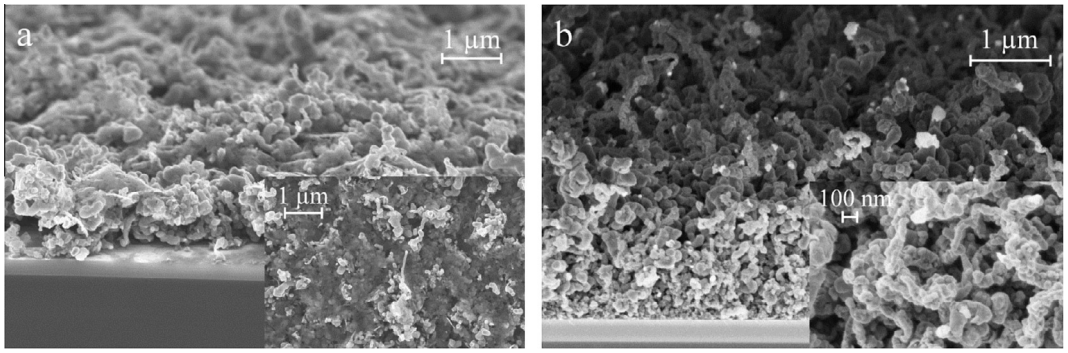

Fig. 3. Cross-sectional SEM images of CNFs grown (1 h, 635 °C, C_2H_4) on (a) reduced 25 nm Ni, and (b) reduced 25 nm Ni/10 nm Ta. The insets show top-views of the samples.

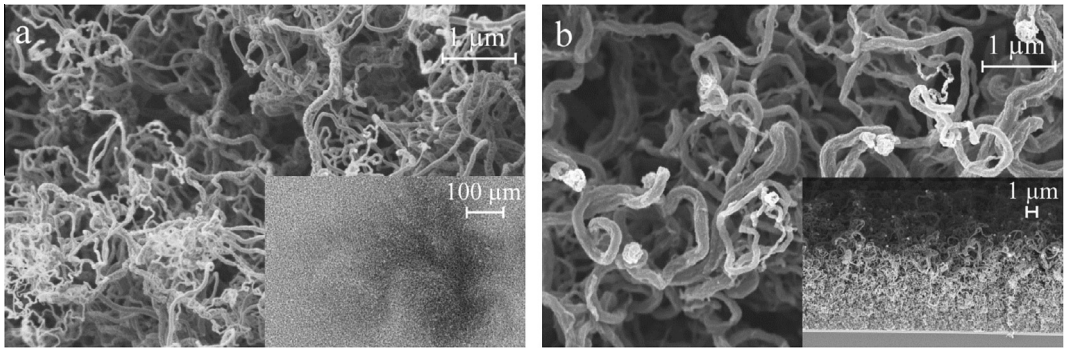

Fig. 4. Top view SEM images of CNFs grown (1 h, 635 °C, C_2H_4/H_2) on 10 nm Ni after (a) oxidation pretreatment (the inset shows an image with a lower magnification) and (b) reduction pretreatment (the inset shows a cross-sectional image).

In fact, even without pretreatment, CNFs were formed on 10 nm Ni with good surface uniformity. However, these fibers were very weakly attached (based on cross-sectional SEM images, not shown). Presumably, addition of hydrogen to ethylene 'induces' the formation of nickel nanoparticles during the first minutes of the CNF-synthesis step, and thus CNF-formation, despite the absence of any thermal pretreatment of the Ni film prior to CNF-synthesis.

CNF-layers formed with an ethylene-hydrogen mixture on oxidation-pretreated 10 nm Ni had a 'wavy appearance' (inset Fig. 4a) due to local detachment of the CNF-layer (poor adhesion), and the CNF-diameters were in the range 50–100 nm. In the case of hydrogen assisted growth on reduction-pretreated Ni (Fig 4b), the adhesion of the CNF-layers was better (less detachment), and the CNF-diameters were larger (100–200 nm). The amount of fibers in Fig. 4b (reduction pretreated) appears slightly lower than the amount of fibers in Fig. 4a (oxidation pretreated). For samples containing 25 nm Ni, similar results were found in terms of growth, adhesion and formation rate of CNFs. In the case of oxidation-pretreatment, thin smooth CNFs (diameter: 50–100 nm) with an apparent high density were formed on Ni and Ni/Ta, while for reduction-pretreatment, thicker CNFs with a (slightly) lower density were observed (diameter ~100 nm on Ni, and ~200 nm on Ni/Ta, respectively). Moreover, Ni/Ta samples contained a broader range of CNF diameters, due to the larger variation in the size of nickel nanoparticles during pretreatment (see Fig. 2b, d, f). CNFs synthesized on Ni/Ta had excellent adhesive properties, significantly better than CNFs on 10 nm or 25 nm Ni-films, independent of the pretreatment conditions.

In conclusion, CNF-synthesis on reduced Ni/Ta thin film samples using C_2H_4/H_2 results in CNF-layers with excellent adhesion to the support and uniform coverage of the surface. With this hydrocarbon source on reduced Ni thin films without Ta CNF-layers can be grown uniformly as well, but these layers suffer from poor adhesion.

3.3. Wettability of synthesized CNF-layers

The wettability of CNF-layers after 1 h of synthesis grown on reduction-pretreated Ni and Ni/Ta samples (synthesis conditions: 635 °C, C_2H_4/H_2) was determined. CNF-layers on 10 nm Ni samples were hydrophobic: contact angles were ca. 138°, whereas for 25 nm Ni, no CA could be determined due to detachment of the CNF-layer. In contrast, CNF-layers on Ni/Ta exhibit CA-values of ~88°. However, although hydrophobic, CNF-layers on Ni-samples had an important disadvantage: the attachment of such CNFs to the oxidized silicon substrate was poor. This was experienced during static CA-measurements: the impact of droplets resulted in partial removal/detachment of the CNF-layers.

It is known that the morphological properties like thickness and porosity of the CNF-layers may influence the wetting behavior [10,11]. In an attempt to get more insight in the influence of the morphological changes during synthesis, the synthesis time of the CNF-layers was varied for reduced nickel-based samples. CNF-layers were grown on reduced Ni and Ni/Ta for various growth times in the range 5–60 min (635 °C, C_2H_4/H_2), and the measured thicknesses (as deduced from cross-sectional SEM images) of the CNF-layers are plotted in Fig. 5a.

In case of samples with Ni only, the CNF-layer thickness increased with time up to 30 min of growth, and the thickness levelled afterwards (10 nm Ni) or even decreased slightly (25 nm Ni). The CNF-layer thickness on Ni/Ta increased up to 25 min of growth, followed by a plateau around 35 µm for longer synthesis times: this is due to deactivation of catalyst particles. Similar

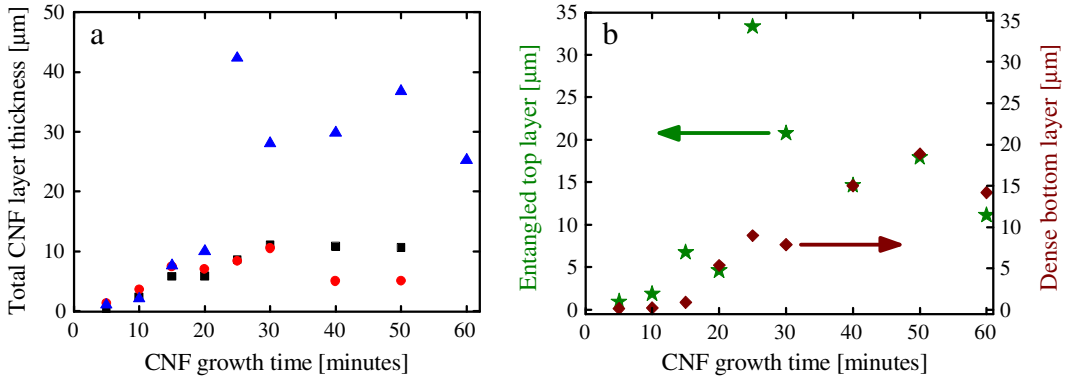

Fig. 5. (a) Total CNF-layer thicknesses as a function of growth time (635 °C, C_2H_4/H_2) after reduction-pretreatment on 25 nm Ni/10 nm Ta (▲), 25 nm Ni (●) and 10 nm Ni (■). (b) Thicknesses of entangled fiber-part at the top (★) and the dense layer at the bottom (♦) as a function of growth time for CNF-layers on Ni/Ta (635 °C, C_2H_4/H_2).

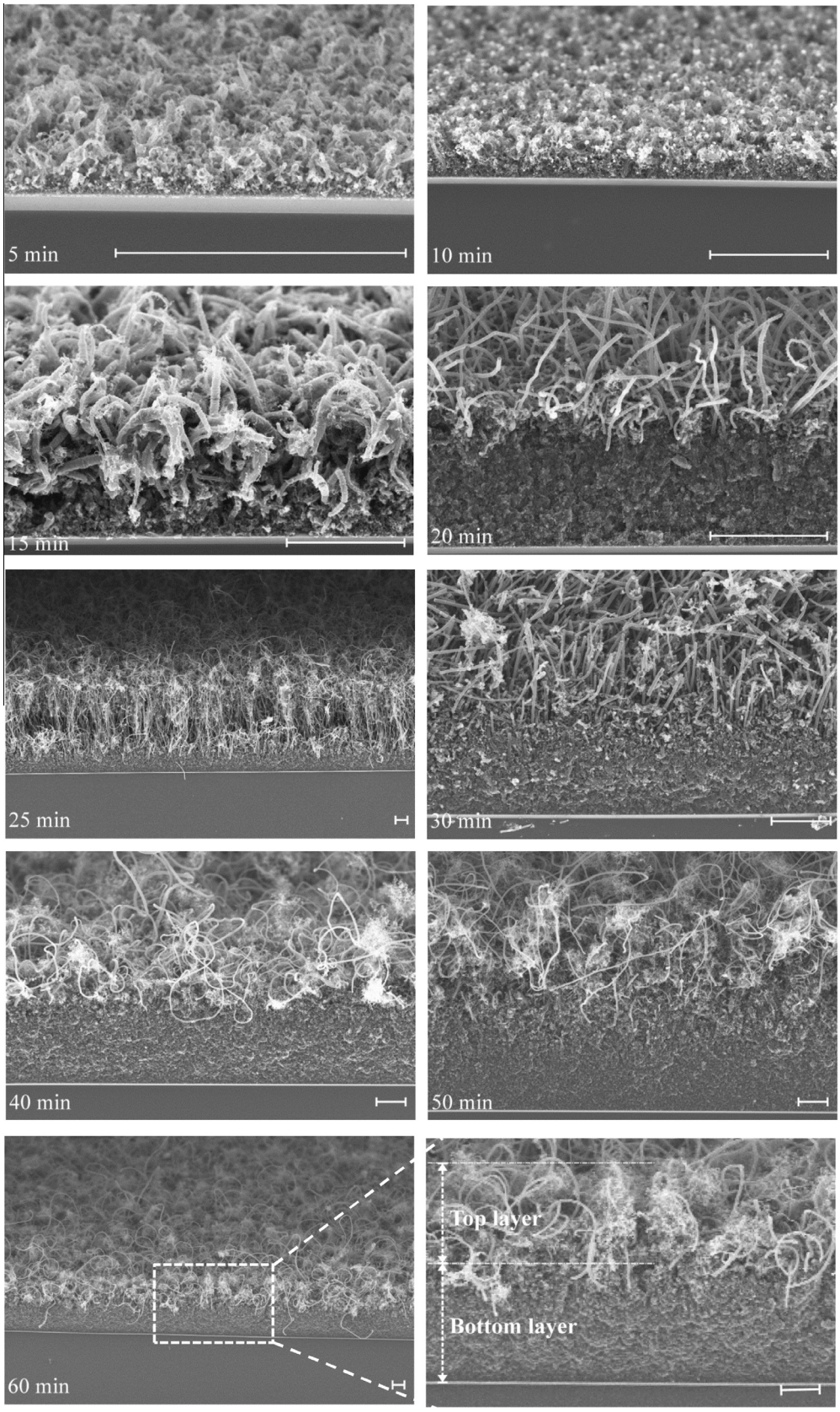

Fig. 6. Cross-sectional SEM images of CNF-layers synthesized (635 °C, C_2H_4/H_2) on reduced Ni/Ta for various growth times. The scale bar corresponds to 5 μm in each image. The top and bottom layers are indicated in the image of the sample grown in 60 min.

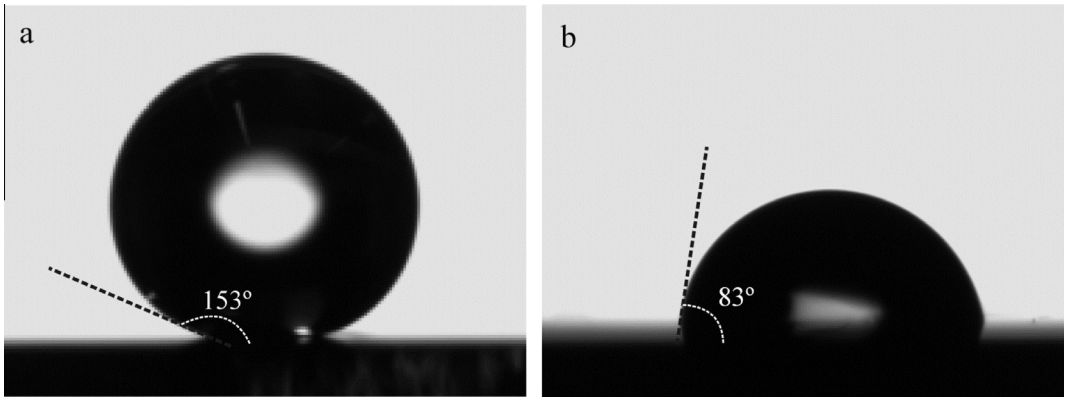

Fig. 7. Photographs of water droplets on as grown (635 °C, C_2H_4/H_2) CNF-layers. After 10 min growth the layer is superhydrophobic (a), while after 50 min growth the layer is hydrophilic (b).

observations were reported for CNF-growth on nickel foams [28]. In addition, careful inspection of the SEM images of the grown CNF-layers on Ni/Ta (Fig. 6) reveals that for growth times of 20–30 min the CNF-layers are more (vertically) aligned, and that for longer synthesis times ($\geqslant$30 min) the CNFs start to curl and intertwine progressively with growth time (which shows up as a reduction in the height of the entangled top layer in Fig. 5b), leading to a densification of the CNF-layer. These effects might contribute to a reduction (25 nm Ni) or levelling (Ni/Ta) of the total layer thickness for growth times above 30 min (Fig. 5a). In addition, small variation in the growth temperature (from run-to-run) might influence the growth kinetics of the CNFs substantially, giving rise to the observed variations in total layer thickness.

CNF-layers on Ni/Ta had excellent adhesion to the support, whereas CNF-layers on Ni were prone to peeling off/detachment for growth times >30 min (the longer the growth time, the worse the attachment of CNFs on Ni samples). A growth time of $\leqslant$15 min is the best for fairly good adhesion of CNF-layers on reduced Ni.

Fig. 6 shows the typical SEM images of CNF-layers synthesized on reduced Ni/Ta for various growth times.

For longer growth-times (>15 min) a "densified" C-layer is recognizable in which no individual fibers can be discriminated (this C-layer is most likely composed of amorphous carbon [35]), with a layer on its top, containing clearly observable, randomly-oriented, entangled CNFs. The bottom layer ("dense" C-layer) and top layer (entangled CNFs) are indicated in the cross sectional SEM images for the sample after 60 min growth in Fig. 6. The adhesion of the CNF layer to the substrate is excellent on these substrates, which is most probably originating from the dense C-layer, which anchors the CNFs firmly to the substrate. The thicknesses of both the entangled fiber-part as well as the dense C-part as a function of growth time are given in Fig. 5b. The thickness of the dense carbon sublayer increases approximately linearly with the growth time, which is not the case for the sublayer of entangled fibers: For growth times above 25 min, the height of the entangled CNF layer decreases to around 18 μm.

In. Fig. 7, characteristic photographs are shown of a droplet on CNF-layers that are superhydrophobic or hydrophilic, as-synthesized on reduced Ni/Ta using two different growth times (10 and 50 min). The CA-values extracted from these photographs are shown in Fig. 8 as a function of the growth time.

For comparison we determined the CA-values of the as evaporated and pretreated substrates prior to CNF growth (see Table 1.) Except for the as evaporated 10 nm Ni substrates, all the contact angles prior to CNF growth are very comparable (94.5° ± 1.5°). The somewhat lower contact angle for the as evaporated 10 nm Ni substrates might arise from a partial coverage of

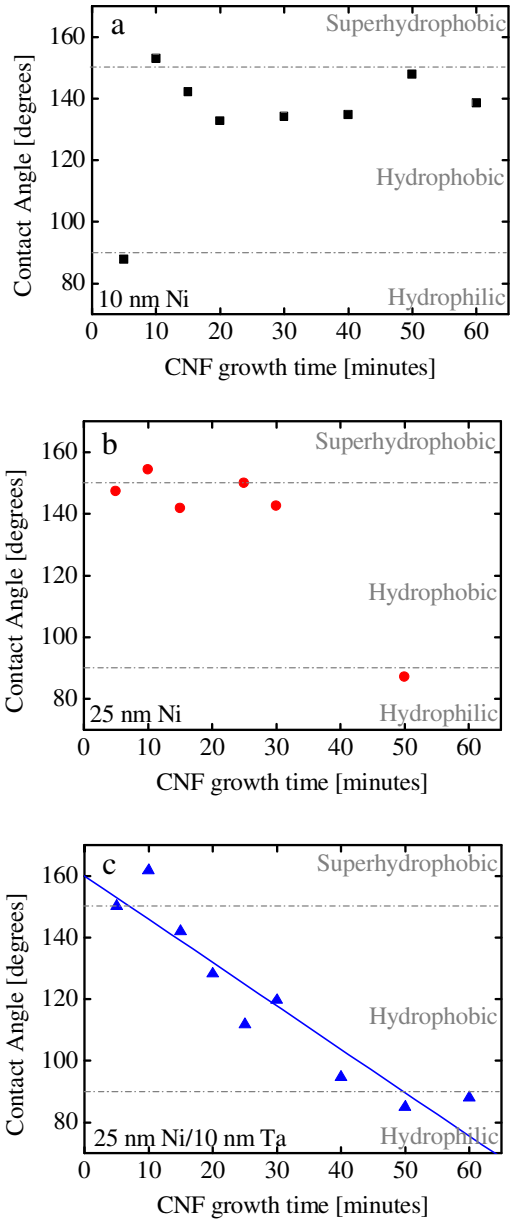

Fig. 8. Contact angle values measured on CNF-layers (635 °C, C_2H_4/H_2) as a function of growth time after reduction-pretreatment on (a) 10 nm Ni (■), (b) 25 nm Ni (●) and (c) 25 nm Ni/10 nm Ta (▲). In (c) a linear trendline is added as a guide to the eyes.

Table 1
Contact angle values of the substrates prior to CNF growth.

Substrate	Treatment	Contact angle (°)
10 nm Ni	As evaporated	78
	Reduced (2 h, 500 °C)	96
25 nm Ni	Oxidized (2 h, 500 °C)	95
	As evaporated	96
25 nm Ni/10 nm Ta	Reduced (2 h, 500 °C)	94
	Oxidized (2 h, 500 °C)	95
	As evaporated	96
	Reduced (2 h, 500 °C)	93
	Oxidized (2 h, 500 °C)	93

the Si surface, hence showing an averaged contact angle between the contact angles on Ni and Si.

As a result of the CNF-growth the CAs change. It can be observed in Fig. 8 that CNF-layers are superhydrophobic for a growth time of 10 min on samples with a "thick" Ni-content (25 nm as-evaporated). More generally, if no Ta is used underneath the Ni, almost all growth times yielded highly hydrophobic CNF-layers with a CA above 130°. It is believed that these high CA-values were maintained because the thickness of the CNF-layer was not increasing significantly for growth times $\geqslant$20 min, most likely due to deactivation of the catalytic nickel nanoparticles, which stopped the formation of carbon fibers. However, for very long synthesis times, the adhesion of these very hydrophobic CNFs to the silicon support became very poor. In contrast, CNF-layers on Ni/Ta showed their excellent adhesion for all growth times, but the wettability of these CNF-layers gradually decreased towards hydrophilic. Thus, only thin CNF-layers – with a thickness of 2–3 μm – that are grown for 10 min on Ni/Ta or Ni are superhydrophobic with good adhesion to the support.

Next we discuss the decreasing contact angle with growth time, observed for the stable CNF-layers grown on Ni/Ta (see Fig. 8). Superhydrophobicity is usually explained by either the Wenzel model, when the liquid wets the surface completely, or by the Cassie-Baxter model when the liquid wets only the top of the surface asperities [9]. Assuming homogeneous chemical properties of the surface, the presence of nanostructures amplifies the wettability of the corresponding flat surfaces in the Wenzel case, since the actual wetted area increases, while in the Cassie-Baxter case, the presence of nanostructures will always result in higher contact angles compared to the corresponding flat surface. In both cases the geometric properties of the surface (in our case the diameter, length, orientation and density of the fibers in the entangled layer) will influence the actually wetted area. Top-view and cross-sectional SEM-images (e.g. Fig. 6) reveal a similar appearance of the top-part of all CNF-layers, i.e. entangled fibers with diameter in the range 50–200 nm, with rather identical void spaces (i.e. no large fluctuations in the surface porosity). The decreasing contact angle with increasing growth time can therefore not be related to a 'simple' (i.e. only based on geometric considerations) Cassie-Baxter state, for which one would need a decreasing surface porosity (and hence roughness) with increasing growth time to reproduce the observed trend. For a Wenzel picture, we keep in mind that during growth, the actual surface per unit flat area increases monotonically. In the Wenzel picture, a decreasing trend, as observed in our data with increasing growth time is associated with a hydrophilic surface and would then start initially with at most a contact angle of 90°. Therefore a 'simple' Wenzel picture is also insufficient to explain the observed trends.

The presence of Ta might change the evolution of the catalytically grown CNF with time compared to the substrates without Ta. One could for instance image that Ta nanoparticles induce a change in the growth mode of the CNFs from initially base growth (see the SEM image after 5 min. in Fig. 6) to more tip growth in the later growth (see the SEM images after 10 and 20 min). Such a change in growth mode is at this moment however, speculation and one would need dedicated *in situ* microscopy to verify this hypothesis.

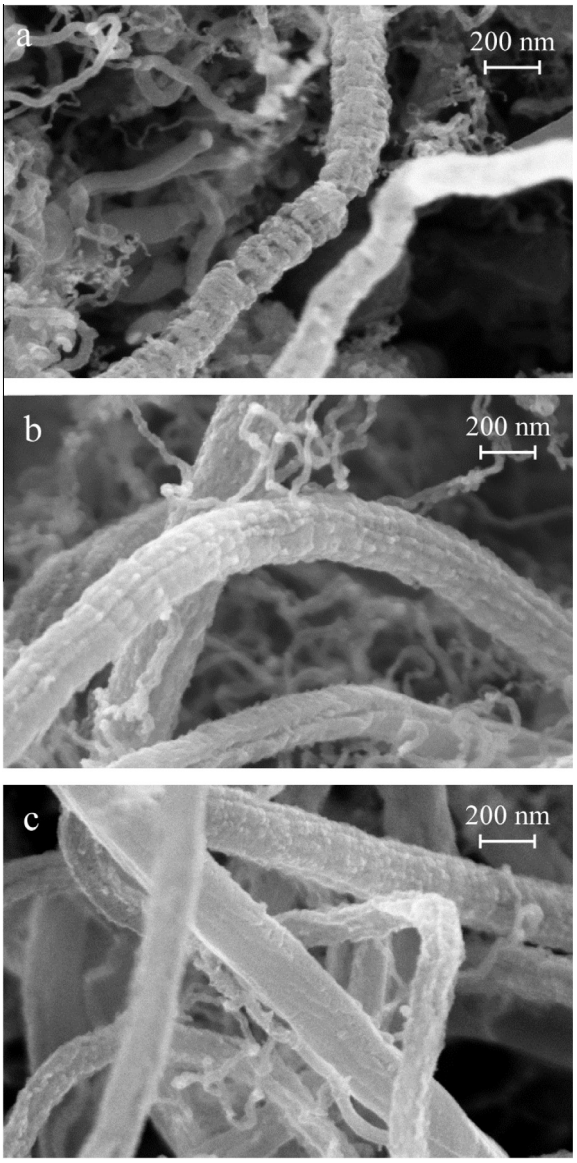

Fig. 9. SEM images of CNFs synthesized on reduced Ni/Ta (1 h, 635 °C, C_2H_4/H_2) for various growth times: (a) 15 min, (b) 40 min and (c) 50 min.

The surface roughness and chemistry of the CNFs may also change during the growth. In Fig. 9 we show representative SEM images of individual CNFs grown on reduced Ni/Ta (1 h, 635 °C, C_2H_4/H_2). It is noticeable that with increasing growth time, the surface roughness of the thicker CNFs decreases, while their diameter increases slightly. These morphological and chemical changes will clearly influence the wetting properties of the CNF surfaces, but further research is needed to investigate and model their exact role.

The apparently decisive role of the CNF-layer thickness in the wettability is also reported in earlier work in our group [25], where, in contrast to our findings here, an increasing contact angle with increasing layer thickness was reported for CNF-layers grown on Ni metal foils. For the CNF-layers grown on polycrystalline Ni foils the surface roughness was reported on the scale of tens of microns [25], while roughness in such dimensions is completely absent on the CNF-layers grown on Ni thin films in this study. In

addition, for the CNF-layers grown on Ni foils it was assumed that the surface chemistry of the CNF did not have a noticeable effect on the wettability of the CNF-layers [25], while in the Ni thin film based CNF layers in this study a decisive role of changes in the surface chemistry cannot be ruled out. These differences in the CNF-layer properties on Ni foils versus Ni thin films might very well be related to the different wetting properties on these layers.

The stability of the superhydrophobicity of the CNF-layers on reduced Ni/Ta was verified by repetitive measurements of the contact angle on the same sample for a period of 36 months. During this period we observed –in contrast to observations on pristine superhydrophobic CNT-samples [36]- no influence of UV irradiation or dark storage on the wettability of the CNF-layers. We did not observe any change in the contact angle over this period. In addition, the contact line of evaporating droplets is strongly pinned on CNF substrates (hysteresis values up to 65° were measured), which, together with the high contact angle, makes these substrates ideally suited for evaporation studies in the constant contact area mode [23].

In summary, on pure-Ni samples (super)hydrophobic CNF-layers can be obtained, however, their attachment to the Si substrate is rather poor, which limits their practical use. For CNF-layers grown on Ni/Ta substrates the adhesion to the Si substrate is excellent and their wettability can be effectively tuned from superhydrophobic to hydrophilic by variation of the growth time.

4. Conclusions and outlook

Various nickel-based thin films – 10 nm Ni, 25 nm Ni and 25 nm Ni/10 nm Ta – on oxidized silicon supports were exposed to an oxidation or reduction pretreatment (2 h, 500 °C) in order to dewet these continuous films into nanoparticles. Ni nanoparticle formation, which is required for CNF-growth, was only observed when a reductive pretreatment was applied. Ni nanoparticle size and distribution depended on the thickness of the nickel film as well as the presence of a tantalum adhesion layer. The nanoparticle size distribution influenced the diameter of the CNFs qualitatively.

On reduced Ni and Ni/Ta thin films CNFs could be TC–CVD synthesized (with uniform surface coverage) using ethylene, and addition of hydrogen enhanced the formation rate of CNF-layers. Whereas the adhesion of CNF-layers on Ni samples was poor (in particular for growth times longer than 30 min), on Ni/Ta the adhesion of CNF-layers was excellent.

Wettability investigations on CNF-layers grown on reduction-pretreated Ni and Ni/Ta (synthesis conditions: 635 °C, C_2H_4/H_2) revealed that CNF layers grown on Ni were (nearly) superhydrophobic for all growth times, whereas the wettability of CNF-layers on Ni/Ta changed gradually from superhydrophobic for growth times $\leqslant$10 min to hydrophilic for growth times $\geqslant$s50 min.

The possibility to tune the wettability of well-adhesive, as-synthesized CNF-layers – no post-synthesis treatments were applied – enables the systematic variation of the wettability in flow channels of silicon-based microfluidic systems by a CNF coating. For example, hydrophilic CNF-layers can be used as catalyst support in microreactors [37,38] and superhydrophobic CNFs as coatings for drag reduction (superlubrification).

Acknowledgements

We gratefully acknowledge M. Smithers (MESA$^+$ Nanolab) for SEM imaging, B. Geerdink for technical support, and the SFI group (University of Twente) for use of their contact-angle meter. AvH gratefully acknowledges NWO for financial support under grant No. 700.10.408. Part of this work was performed with the financial support from the MicroNed program, under cluster-II of Smart Microchannel technology (SMACT) and workpackage II-G-2 and 3 (Smart Micro Reactors).

References

[1] X.J. Feng, L. Jiang, Design and creation of superwetting/antiwetting surfaces, Adv. Mater. 18 (2006) 3063.
[2] S.T. Yohe, Y.L. Colson, M.W. Grinstaff, Superhydrophobic materials for tunable drug release: using displacement of air to control delivery rates, J. Am. Chem. Soc. 134 (2012) 2016.
[3] R. Blossey, Self-cleaning surfaces – virtual realities, Nat. Mater. 2 (2003) 301.
[4] A.J. Meuler, G.H. McKinley, R.E. Cohen, Exploiting topographical texture to impart icephobicity, ACS Nano 4 (2010) 7048.
[5] G. McHale, M.I. Newton, N.J. Shirtcliffe, Immersed superhydrophobic surfaces: Gas exchange, slip and drag reduction properties, Soft Matter 6 (2010) 714.
[6] P. Joseph, C. Cottin-Bizonne, J.-M. Benoît, C. Ybert, C. Journet, P. Tabeling, L. Bocquet, Slippage of water past superhydrophobic carbon nanotube forests in microchannels, Phys. Rev. Lett. 97 (2006) 156104.
[7] H.C. Aran, J.K. Chinthaginjala, R. Groote, T. Roelofs, L. Lefferts, M. Wessling, R.G.H. Lammertink, Porous ceramic mesoreactors: A new approach for gas-liquid contacting in multiphase microreaction technology, Chem. Eng. J. 169 (2011) 239.
[8] L. Bocquet, E. Charlaix, Nanofluidics, from bulk to interfaces, Chem. Soc. Rev. 39 (2010) 1073.
[9] D. Quéré, Wetting and roughness, Annu. Rev. Mater. Res. 38 (2008) 71.
[10] D. Öner, T.J. McCarthy, Ultrahydrophobic surfaces. effects of topography length scales on wettability, Langmuir 16 (2000) 7777.
[11] M. Ma, R.M. Hill, Superhydrophobic surfaces, Curr. Opin. Colloid Interface Sci. 11 (2006) 193.
[12] A. Nakajima, K. Hashimoto, T. Watanabe, K. Takai, G. Yamauchi, A. Fujishima, Transparent superhydrophobic thin films with self-cleaning properties, Langmuir 16 (2000) 7044.
[13] H. Liu, J. Zhai, L. Jiang, Wetting and anti-wetting on aligned carbon nanotube films, Soft Matter 2 (2006) 811.
[14] J.H. Bitter, Nanostructured carbons in catalysis a Janus material - industrial applicability and fundamental insights, J. Mater. Chem. 20 (2010) 7312.
[15] K.K.S. Lau, J. Bico, K.B.K. Teo, M. Chhowalla, G.A.J. Amaratunga, W.I. Milne, G.H. McKinley, K.K. Gleason, Superhydrophobic carbon nanotube forests, Nano Lett. 3 (2003) 1701.
[16] B.A. Kakade, V.K. Pillai, Tuning the wetting properties of multiwalled carbon nanotubes by surface functionalization, J. Phys. Chem. C 112 (2008) 3183.
[17] S.M.C. Journet, C. Ybert, S.T. Purcell, L. Bocquet, Contact angle measurements on superhydrophobic carbon nanotube forests: Effect of fluid pressure, Europhys. Lett. 71 (2005) 104.
[18] T. Sun, H. Liu, W. Song, X. Wang, L. Jiang, L. Li, D. Zhu, Responsive aligned carbon nanotubes, Angew. Chem. 116 (2004) 4763.
[19] Z. Wang, L. Ci, L. Chen, S. Nayak, P.M. Ajayan, N. Koratkar, Polarity-dependent electrochemically controlled transport of water through carbon nanotube membranes, Nano Lett. 7 (2007) 697.
[20] L. Zhang, D.E. Resasco, Single-walled carbon nanotube pillars: A superhydrophobic surface, Langmuir 25 (2009) 4792.
[21] G.W.T. Sun, H. Liu, L. Feng, D. Zhu, Control over the wettability of an aligned carbon nanotube film, J. Am. Chem. Soc. 125 (2003) 14996.
[22] K. Gjerde, R.T.R. Kumar, K.N. Andersen, J. Kjelstrup-Hansen, K.B.K. Teo, W.I. Milne, C. Persson, K. Molhave, H.-G. Rubahn, P. Boggild, On the suitability of carbon nanotube forests as non-stick surfaces for nanomanipulation, Soft Matter 4 (2008) 392.
[23] H. Gelderblom, Á.G. Marín, H. Nair, A. van Houselt, L. Lefferts, J.H. Snoeijer, D. Lohse, How water droplets evaporate on a superhydrophobic substrate, Phys. Rev. E 83 (2011) 026306.
[24] P. Tsai, S. Pacheco, C. Pirat, L. Lefferts, D. Lohse, Drop impact upon micro- and nanostructured superhydrophobic surfaces, Langmuir 25 (2009) 12293.
[25] S. Pacheco Benito, L. Lefferts, Wettability of carbon nanofiber layers on nickel foils, J. Colloid Interface Sci. 364 (2011) 530.
[26] D.B. Thakur, R.M. Tiggelaar, J.G.E. Gardeniers, L. Lefferts, K. Seshan, Growth of carbon nanofiber coatings on nickel thin films on fused silica by catalytic thermal chemical vapor deposition: On the use of titanium, titanium–tungsten and tantalum as adhesion layers, Surf. Coat. Technol. 203 (2009) 3435.
[27] R.M. Tiggelaar, D.B. Thakur, H. Nair, L. Lefferts, K. Seshan, J.G.E. Gardeniers, Influence of thin film nickel pretreatment on catalytic thermal chemical vapor deposition of carbon nanofibers, submitted to Thin Solid Films.
[28] N.A. Jarrah, J.G. van Ommen, L. Lefferts, Mechanistic aspects of the formation of carbon-nanofibers on the surface of Ni foam: A new microstructured catalyst support, J. Catal. 239 (2006) 460.
[29] P.D. Rack, Y. Guan, J.D. Fowlkes, A.V. Melechko, M.L. Simpson, Pulsed laser dewetting of patterned thin metal films: A means of directed assembly, Appl. Phys. Lett. 92 (2008) 223108.
[30] S.J. Randolph, J.D. Fowlkes, A.V. Melechko, K.L. Klein, H.M. Meyer III, M.L. Simpson, P.D. Rack, Controlling thin film structure for the dewetting of catalyst nanoparticle arrays for subsequent carbon nanofiber growth, Nanotechnol. 18 (2007) 465304.

[31] J.D. Carey, L.L. Ong, S.R.P. Silva, Formation of low-temperature self-organized nanoscale nickel metal islands, Nanotechnol. 14 (2003) 1223.
[32] D.B. Thakur, R.M. Tiggelaar, J.G.E. Gardeniers, L. Lefferts, K. Seshan, Silicon based microreactors for catalytic reduction in aqueous phase: use of carbon nanofiber supported palladium catalyst, Chem. Eng. J. 227 (2013) 128.
[33] R.T.K. Baker, Catalytic growth of carbon filaments, Carbon 27 (1989) 315.
[34] J.K. Chinthaginjala, L. Lefferts, Influence of hydrogen on the formation of a thin layer of carbon nanofibers on Ni foam, Carbon 47 (2009) 3175.
[35] D.B. Thakur, R.M. Tiggelaar, J.G.E. Gardeniers, L. Lefferts, K. Seshan, Carbon nanofiber based catalyst supports to be used in microreactors: Synthesis and characterization, Chem. Eng. J. 160 (2010) 899.
[36] J. Yang, Z. Zhang, X. Men, X. Xu, X. Zhu, Reversible superhydrophobicity to superhydrophilicity switching of a carbon nanotube film via alternation of UV irradiation and dark storage, Langmuir 26 (2010) 10198.
[37] D.B. Thakur, R.M. Tiggelaar, T.M.C. Hoang, J.G.E. Gardeniers, L. Lefferts, K. Seshan, Ruthenium catalyst on carbon nanofiber support layers for use in silicon-based structured microreactors. Part I: Preparation and characterization, Appl. Catal. B 102 (2011) 232.
[38] D.B. Thakur, R.M. Tiggelaar, Y. Weber, J.G.E. Gardeniers, L. Lefferts, K. Seshan, Ruthenium catalyst on carbon nanofiber support layers for use in silicon-based structured microreactors. Part II: Catalytic reduction of bromate contaminants in aqueous phase, Appl. Catal. B 102 (2011) 243.